EUROPEAN ORGANIZATION FOR NUCLEAR RESEARCH

Memorandum of the NA49 Collaboration to the SPSC

Status and further Analysis Plans of the NA49 Collaboration

T. Anticic[22], B. Baatar[8], D. Barna[4], J. Bartke[6], H. Beck[9], L. Betev[10], H. Białkowska[19], C. Blume[9], B. Boimska[19], J. Book[9],, M. Botje[1], J. Bracinik[3], P. Bunčić[10], V. Cerny[3], P. Christakoglou[1], P. Chung[18], O. Chvala[14], J.G. Cramer[15], P. Csató[4], P. Dinkelaker[9], V. Eckardt[13], H.G. Fischer[10], Z. Fodor[4], P. Foka[7], V. Friese[7], J. Gál[4], M. Gaździcki[9,11], V. Genchev[17], K. Grebieszkow[21], S. Hegyi[4], C. Höhne[7], K. Kadija[22], A. Karev[13], V.I. Kolesnikov[8], M. Kowalski[6], M. Kreps[3], A. Laszlo[4], R. Lacey[18], M. van Leeuwen[1], P. Lévai[4], L. Litov[16], M. Makariev[16], A.I. Malakhov[8], M. Mateev[16], M. Mackowiak[21], G.L. Melkumov[8], M. Mitrovski[9], J. Molnár[4], St. Mrówczyński[11], V. Nicolic[22], G. Pálla[4], A.D. Panagiotou[2], D. Panayotov[16], W. Peryt[21], M. Pikna[3], J. Pluta[21], D. Prindle[15], F. Pühlhofer[12], R. Renfordt[9], C. Roland[5], G. Roland[5], M. Rybczyński[11], A. Rybicki[6], A. Sandoval[7], N. Schmitz[13], T. Schuster[9], P. Seyboth[13], F. Siklér[4], B. Sitar[3], E. Skrzypczak[20], M. Slodkowski[21], G. Stefanek[11], R. Stock[9], H. Ströbele[9], T. Susa[22], I. Szentpétery[4], J. Sziklai[4], M. Szuba[21], P. Szymanski[10,19], M. Utvic[9], D. Varga[4,10], M. Vassiliou[2], G.I. Veres[4,5], G. Vesztergombi[4], D. Vranić[7], S. Wenig[10], Z. Włodarczyk[11], A. Wojtaszek[11]

[1]NIKHEF, Amsterdam, Netherlands.
[2]Department of Physics, University of Athens, Athens, Greece.
[3]Comenius University, Bratislava, Slovakia.
[4]KFKI Research Institute for Particle and Nuclear Physics, Budapest, Hungary.
[5]MIT, Cambridge, USA.
[6]Henryk Niewodniczanski Institute of Nuclear Physics, Polish Academy of Sciences, Cracow, Poland.
[7]Gesellschaft für Schwerionenforschung (GSI), Darmstadt, Germany.
[8]Joint Institute for Nuclear Research, Dubna, Russia.
[9]Fachbereich Physik der Universität, Frankfurt, Germany.
[10]CERN, Geneva, Switzerland.
[11]Institute of Physics, Jan Kochanowski University, Kielce, Poland.
[12]Fachbereich Physik der Universität, Marburg, Germany.
[13]Max-Planck-Institut für Physik, Munich, Germany.
[14]Charles University, Faculty of Mathematics and Physics, Institute of Particle and Nuclear Physics, Prague, Czech Republic.
[15]Nuclear Physics Laboratory, University of Washington, Seattle, WA, USA.
[16]Atomic Physics Department, Sofia University St. Kliment Ohridski, Sofia, Bulgaria.
[17]Institute for Nuclear Research and Nuclear Energy, Sofia, Bulgaria.
[18]Department of Chemistry, Stony Brook Univ. (SUNYSB), Stony Brook, USA.
[19]Institute for Nuclear Studies, Warsaw, Poland.

CERN-SPSC-2009-033 / SPSC-SR-052
23/09/2009

[20]Institute for Experimental Physics, University of Warsaw, Warsaw, Poland.
[21]Faculty of Physics, Warsaw University of Technology, Warsaw, Poland.
[22]Rudjer Boskovic Institute, Zagreb, Croatia.

1 Introduction

The main aim of the NA49 experiment is the study of hadronic matter at highest temperatures and densities in Pb+Pb collisions in search for the onset of quark-gluon deconfinement and the QCD predicted critical point of strongly interacting matter. In addition, p+p and p+A reactions are investigated in order to elucidate the particle production mechanism in elementary collisions and to study the effects of cold nuclear matter on particle production yields.

Although the last data of NA49 was taken in 2002, the analysis of the rich accumulated data set continues by numerous students and senior physicists. This is of particular interest for the physics program of the NA61 experiment wich will extend the systematic study of nucleus-nucleus reactions performed by NA49 (mainly Pb+Pb collisions) by investigating reactions of medium-size (A $\approx$ 130 and 30) as well as light (A $\approx$ 12) nuclei. In this context, NA49 provides the heavy nucleus reference and offers valuable analysis experience for the physicists which will form the core of the NA61 analysis team.

This report discusses the analysis progress since the last submitted status report of 2008 [1] and presents the requests to CERN for the continuing work of the NA49 collaboration. Furthermore, we inform the SPSC that the former NA49 detector has been formally transferred to the NA61 collaboration with a memorandum of understanding between CERN and the NA61 and NA49 collaborations.

2 Publications in refereed journals since October 2008

- Energy dependence of multiplicity fluctuations in heavy ion collisions at 20A to 158A GeV
  C. Alt et al., Phys.Rev. C78, 034914 (2008).
- Energy dependence of Λ and Ξ production in central Pb+Pb collisions at 20A, 30A, 40A, 80A, and 158A GeV measured at the CERN Super Proton Synchrotron
  C. Alt et al., Phys.Rev. C78, 034918 (2008).
- Energy dependence of Φ meson production in central Pb+Pb collisions at $\sqrt{s_{NN}}$ = 6 to 17 GeV
  C. Alt et al., Phys.Rev. C78, 044907 (2008).
- Energy dependence of transverse momentum fluctuations in Pb+Pb collisions at the CERN Super Proton Synchrotron (SPS) at 20A to 158A GeV
  T. Anticic et al., Phys.Rev. C79, 044904 (2009).
- Energy dependence of particle ratio fluctuations in central Pb + Pb collisions from $\sqrt{s_{NN}}$ = 6.3 to 17.3 GeV
  C. Alt et al., Phys.Rev. C79, 044910 (2009).

3 Submitted for publication

- System-size dependence of Λ and Ξ production in nucleus-nucleus collisions at 40A and 158A GeV measured at the CERN Super Proton Synchrotron
  T. Anticic et al., preprint arXiv:0906.0469 (2009), accepted Phys.Rev.C.
- Inclusive production of protons, anti-protons and neutrons in p+p collisions at 158 GeV/c beam momentum
  T. Anticic et al., preprint arXiv:0906:4488 (2009), submitted Eur.Phys.J.C.
- Three-dimensional two-pion source image from Pb+Pb collisions at $\sqrt{s_{NN}}$ = 17.3 GeV: new constraints for source breakup dynamics

C. Alt et al., submitted Phys.Lett.B.

4 Publication drafts under review in the collaboration:

- Production of Λ, $\bar{\Lambda}$, Ξ, $\bar{\Xi}$, Ξ_{1530}, $\bar{\Xi}_{1530}$, Ω and $\bar{\Omega}$ in p+p interactions at 158 GeV/c
- Centrality dependence of (anti-)proton spectra in Pb+Pb collisions at $40A$ and $158A$ GeV measured at the CERN SPS
- $K^*(892)^0$ and $\bar{K}^*(892)^0$ production in central Pb+Pb collisions at $158A$ GeV
- Search for the QCD critical point in nuclear collisions at the CERN SPS

5 Subjects of current analyses:

5.1 p+p and p+A reactions:

5.1.1 Analysis work of the Bratislava, Budapest, Krakow, CERN, Oxford, Prague, Sofia groups

- Charged kaon production in p+p interactions at 158 GeV/c beam momentum; detailed comparison with existing data and discussion of s-dependence from threshold to collider energies
- Charged kaons, protons and anti-protons in p+C interactions at 158 GeV/c beam momentum and comparison to the corresponding p+p interactions
- Charged pion production in p+Pb interactions at 158 GeV/c beam momentum in 5 centrality bins including a detailed comparison to p+p interactions
- Charged kaon, proton and anti-proton production in p+Pb interactions at 158 GeV/c beam momentum in 5 centrality bins including a detailed comparison to p+p interactions
- Final state Coulomb interaction in nuclear reactions

5.1.2 Analysis work of the Zagreb group

- production of K^0_S, hyperons and hyperon resonances in p+p and p+Pb collisions (T. Anticic, V. Nicolic, T. Susa)

5.2 Pb+Pb reactions:

- Centrality dependence of pion and kaon production in Pb+Pb collisions at $40A$ and $158A$ GeV (P. Dinkelaker, C. Höhne)
- Energy dependence of azimuthal angle fluctuations using the observable Φ_ϕ in Pb+Pb collisions (K. Grebieszkow, T. Cetner)
- Multiplicity fluctuations in p+p and p+Pb reactions (M. Rybczynski)
- Energy and system size dependence of hadron ratio fluctuations (D. Kresan, C. Höhne, T. Schuster, R. Stock)
- Correlations of $\langle p_T \rangle$ and charged particle multiplicity (A. Wojtaszek)
- Continuation of the study of hadron ratio fluctuations In Pb+Pb collisions using improved methods (M. Mackowiak)
- Centrality dependence of Φ meson production in Pb+Pb collisions at $40A$ and $158A$ GeV (V. Friese)
- Energy dependence of p and $\bar{\mathrm{p}}$ production in central Pb+Pb collisions from $20A$ to $158A$ GeV at the CERN SPS (M. Kowalski)
- Antideuteron production in Pb+Pb collisions at the CERN SPS (V. Kolesnikov)

- Light nuclei production (^{3}He and t) in Pb+Pb collisions from 20A to 158A GeV at the CERN SPS (V. Kolesnikov)
- Production of ρ^0 in Pb+Pb reactions (W. Borowski)
- Azimuthal correlations at high p_T in 158A GeV Pb+Pb collisions (M. Szuba)
- Proton-Λ correlations in Pb+Pb collisions at 158A GeV (H. Beck)
- K^0_S yields in Pb+Pb collisions (J. Book)
- Wounded nucleon and wounded quark scaling of particle production from nuclear collisions (B. Boimska, H. Bialkowska)
- Coulomb repulsion in Pb+Pb collisions (A. Rybicki)

6 Examples of results from papers recently submitted for publication or under final collaboration review

6.1 Imaging of the pion source

Bose-Einstein correlations of identical pion pairs have been used extensively to obtain information on the space-time properties of their source in particle production reactions. NA49 published a comprehensive analysis using the conventional method of Gaussian fits to the correlation functions and the interpretation of the extracted radius parameters in terms of a blast wave model [2]. An alternative method of source imaging was proposed more recently [3] which does not require assumptions on the functional shape of the correlation function, but rather extracts the source density in a model independent manner by an inversion procedure. Such an analysis has now been performed by NA49 for low transverse momentum identical pion pairs in central Pb+Pb collisions. The result is shown in Fig. 1 demonstrating that the source is not well described by an ellipsoid and shows stronger intensity at large radii in the outward and longitudinal (beam) directions. A comparison with the THERMINATOR model suggests that pions are emitted from the surface of the fireball which shrinks with time.

6.2 System size dependence of p, $\bar{\text{p}}$ and hyperon production

The NA49 analysis of inclusive particle yields first concentrated on measurements of their energy dependence in central Pb+Pb collisions. The results provided evidence that the onset of quark-gluon deconfinement first appears in the early dense stage of the fireball starting at the low energy region of the SPS around 30A GeV [4]. Recent work complements these results with measurements of the collision centrality dependence of yields.

A paper on the sytem size dependence of hyperon production [5] has been accepted for publication in Physical Review C. As an example, rapidity distributions of Λ and $\bar{\Lambda}$ hyperons in 158A GeV Pb+Pb collisons are shown in Fig. 2 for various intervals of centrality (quantified by the number of wounded nucleons (participant nucleons) N_W). A flat distribution is observed for Λ and a Gaussian shape is seen for $\bar{\Lambda}$ hyperons with no significant change from peripheral to central collisions.

The trivial dependence of the yield on the number of nucleons partcipating in the collisions is removed by normalising to the average number of wounded nucleons $\langle N_W \rangle$ for each rapidity interval. The results for the mid-rapidity density at 40A and 158A GeV is plotted in Fig. 3 (top) versus $\langle N_W \rangle$. A moderate rise is seen for Λ and Ξ^- while there is a slight decrease for $\bar{\Lambda}$. One does not find the strong decrease for the latter which might be naively expected due to absorption (annihilation) in the dense fireball of inceasing size. The models HSD and UrQMD2.3 provide a reasonable description of the Λ and $\bar{\Lambda}$ results. However, the yields of Ξ^-

are much larger than predicted by the models. Fig. 3 also displays a long-standing discrepancy of the results of NA49 and NA57 which could not be cleared up in intensive discussions; the resolution of the discrepancy has to be left to future experiments, notably the RHIC low-energy scan.

Total yields of Λ and $\bar{\Lambda}$, normalised to $\langle N_W \rangle$ are presented in Fig. 3 (bottom). The dependence on collision centrality is similar to that for dN/dy. A good description of both is obtained with the core-corona model, which assumes a superposition of nucleon-nucleon like collisions for the outer region and of central Pb+Pb collisions for the inner region of the fireball.

The difference of rapidity spectra of baryons and antibaryons can provide information on the fraction of energy of the incident nucleon energy converted into particle production and on the mechanism of this process. The main features are expected to be exhibited by proton and antiproton yields which have now been extracted as a function of rapidity and collision centrality. The results were written up in a publication draft from which a few sample plots will now be discussed.

The rapidity spectra for protons at $40A$ and $158A$ GeV and for antiprotons at $158A$ GeV in Pb+Pb collisions of 5 centrality classes are displayed in Fig. 4. At $158A$ GeV the proton spectra are parabola shaped and the antiproton spectra exhibit a Gaussian shape with little dependence on the centrality of the collision. At $40A$ GeV the proton spectra change from parabolic to dip structure when proceeding from peripheral to central collisions. The small yield of antiprotons did not allow the extraction of spectra at the lower energy.

Both the parabolic shape of the spectra and the acceptance of elastically or diffractively produced protons (particularly at $40A$ GeV) make it impossible to estimate total inelastic inclusive yields. On the other hand, this is not a problem for antiprotons due to their Gaussian spectrum. As seen from Fig. 5 the $\bar{\mathrm{p}}$ yield per wounded nucleon initially decreases from p+p to peripheral Pb+Pb collisions and then stays constant as for $\bar{\Lambda}$. Again the naively expected absorption is not in evidence.

Finally, Fig. 6 shows a comparison of the measured net-proton rapidity spectra in Pb+Pb reactions to model calculations. Increasing discrepancies develop from peripheral to central collisions, particularly at high absolute values of rapidity.

6.3 $K^*(892)^0$ production in central Pb+Pb collisions at 158A GeV

The high-density state created in Pb+Pb collisions evolves into a hadron-resonance gas which finally decouples into the observed hadrons. The $K^*(892)$ and $\bar{K}^*(892)$ resonance states contain an $\bar{s}$ and s valence quark, respectively, and are therefore sensitive to the level of strangeness production. However, resonance states have finite lifetimes and may interact in the dense medium in which they are produced. Their mass and width could be affected. Scattering processes might destroy or regenerate them. Furthermore, daughters of those K^* that decay inside the fireball may rescatter resulting in a changed invariant mass spectrum. Thus the yields contained in the K^* mass peak were conjectured to be sensitive to the duration and properties of the hadronic fireball stage.

In spite of the huge combinatorial background it was possible to extract a K^* signal in central Pb+Pb collisions at $158A$ GeV. The combinatorial background subtracted mass distribution is shown in Fig. 7 (left). It was fitted with a poynomial background and a Breit-Wigner shape to determine the mass, width and the content of the K^* peak. As can be seen in Fig. 7 (right) the mass value seems to be shifted downward from the world average by, however, only less than twice the systematic uncertainty whereas the width agrees.

The efficiency corrected rapidity distribution is plotted in Fig. 8 (left) from which the

total yield is obtained via a Gaussian fit. Also shown is a calculation using the UrQMD2.3 model which is seen to provide a good description of the experimental result. A comparison of the total $K^*(892)^0$ yield obtained in p+p, C+C, Si+Si and central Pb+Pb collisions normalised to the number of wounded nucleons $\langle N_W \rangle$ to that predicted by the statistical hadron gas model (with parameters fitted without using the $K^*(892)^0$ yield) is presented in Fig. 8 (center). One observes that the yield is suppressed with respect to the model expectation in Pb+Pb reactions. An inspection of the UrQMD2.3 calculation suggests that this seems to be due to an excess of destruction over regeneration of the $K^*(892)^0$ in the fireball. Fig. 8 (right), in which the ratios of measured yields to those predicted by the statistical model are compared for $K^*(892)^0$, $\Lambda(1520)$ and Φ, suggests that the suppression increases with decreasing lifetime of the resonance state.

6.4 Hyperon production in p+p collisions at 158 GeV/c

Published data on hyperon production in p+p collisions are quite incomplete, in particular results for multistrange hyperons are scarce and phase space coverage of transverse momentum, rapidity and Feynman x_F is patchy. Detailed knowledge of p+p collisions is required for a better understanding of elementary collisions as well as for the calibration of models which are used to predict yields in p+A and A+A collisions in order to check for the presence of novel production mechanisms.

Improved geometry calibration and distortion correction procedures led to significantly better reconstruction efficiencies for hyperons. The reanalysis of the full NA49 data sample of $8.2 \cdot 10^6$ p+p collision events has recently been completed and in the following paragraphs a few examples from the results contained in an imminent publication will be presented.

The invariant mass distributions for Ω and $\bar{\Omega}$ candidates are displayed in Fig. 9. In spite of the large event statistics, the number of Ω candidates is only about 70 implying large statistical errors on rapdity and transverse momentum distributions. Using the reanalysed events the previously reported indication of the Ξ^{--} pentaquark candidate [7] was revisited. Although the number of Ξ^- candidates increased the number of pentaquark candidates did not. The NA61 experiment will take an order of magnitude more p+p collision events and should thus be able to provide a definitive answer on the question of its existence.

Fully corrected inclusive cross sections as well as rapdity, Feynman x_F and transverse momentum distributions were obtained. For Λ and $\bar{\Lambda}$ the measurements of NA49 are compared to results available in the literature in Fig. 10. Good consistency is observed.

Rapidity distributions are plotted in Fig. 11 for Λ and $\bar{\Lambda}$, in Fig. 12 for Ξ and $\bar{\Xi}$, and in Fig. 13 for $\Xi(1530)$ and Ω production in inelastic p+p collisions at 158 GeV/c. The experimental results are compared to several model predictions where available (Λ, $\bar{\Lambda}$, Ξ, $\bar{\Xi}$). These are seen to disagree considerably with the data demonstrating the importance of the present measurements for the adjustment of the models and the understanding of the particle production mechanisms in p+p collisions.

7 Requests to CERN

The NA49 collaboration will continue an extensive analysis program with a considerable number of students and senior physicists at least until the end of 2011 when nucleus-nucleus collision data from NA61 are expected to become available. To facilitate this work we request support from the CERN IT division at the level of 35 KSI2000 units in lxbatch. These resources are required for the simulation work connected with determining corrections during the physics

analysis. This work has to use raw data which are stored on the CASTOR system. In addition, we request to keep the presently assigned office space. It is shared with the NA61 collaboration to which the majority of NA49 groups also belong.

References

[1] T. Anticic et al., *Status and further Analysis Plans of the NA49 collaboration*, CERN-SPSC-2008-024.

[2] C. Alt et al., Phys. Rev. **C77**, 064908 (2008).

[3] D. Brown and P. Danielewicz, Phys. Rev. **C64**, 14902 (2001).

[4] C. Alt et al., Phys. Rev. **C77**, 024903 (2008).

[5] T. Anticic et al., preprint arXiv:0906.0469 (2009).

[6] T. Anticic et al., preprint arXiv:0906.4488 (2009).

[7] C. Alt et al., Phys. Rev. Lett. **92**, 042003 (2004).

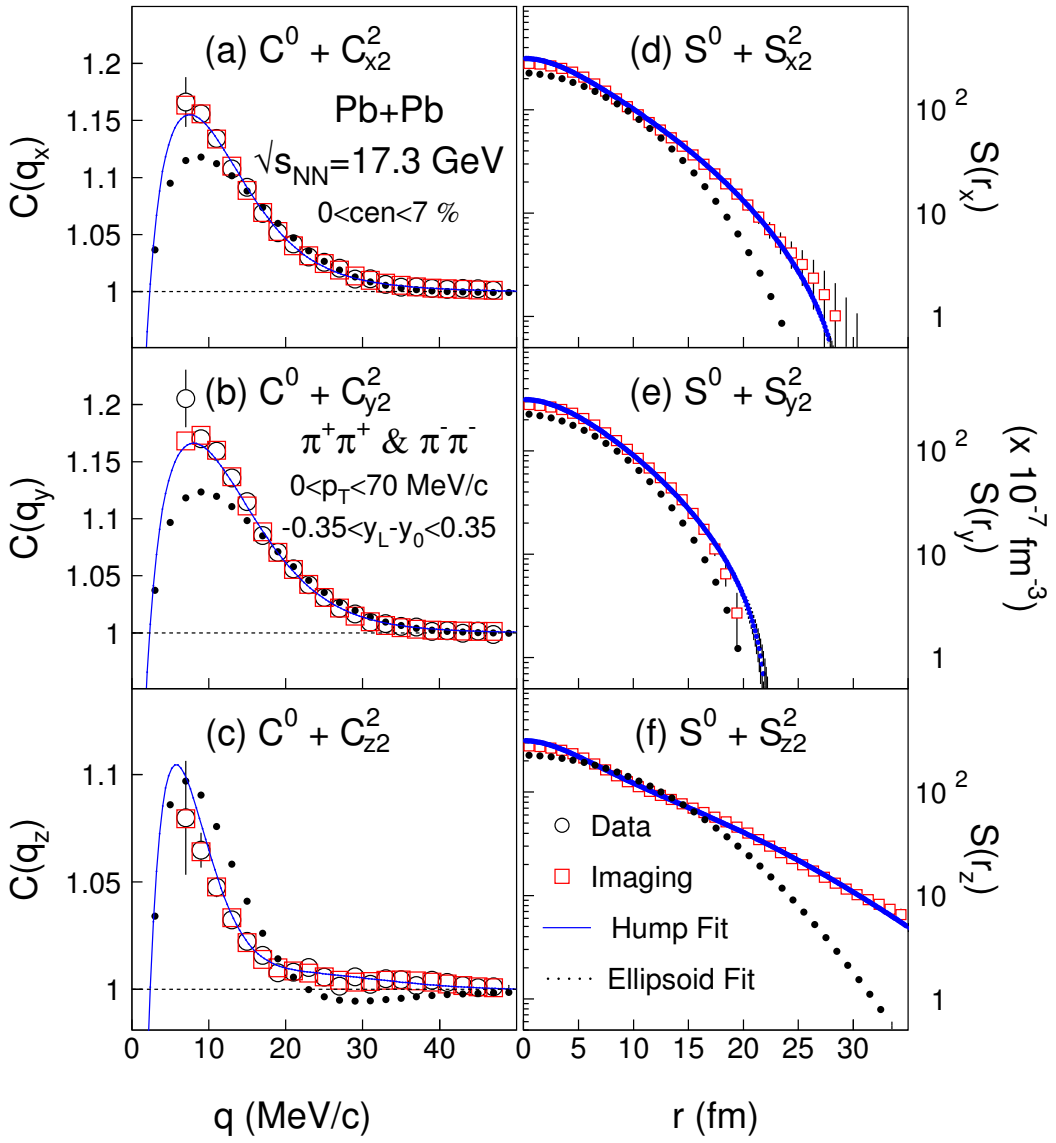

Figure 1: Correlation functions, C(q_i) (left panels), and source functions, S(r_i) (right panels), for $\pi^+\pi^+$ and $\pi^-\pi^-$ pairs in central Pb+Pb collisions at 158A GeV in the outward x (top), sideward y (middle) and longitudinal (bottom) directions. Open circles show the measurements, squares the the imaged source and the correlation corresponding to the imaged source. The dotted and solid lines represent, respectively, the fitted ellipsoid and "hump" sources and their corresponding correlation functions.

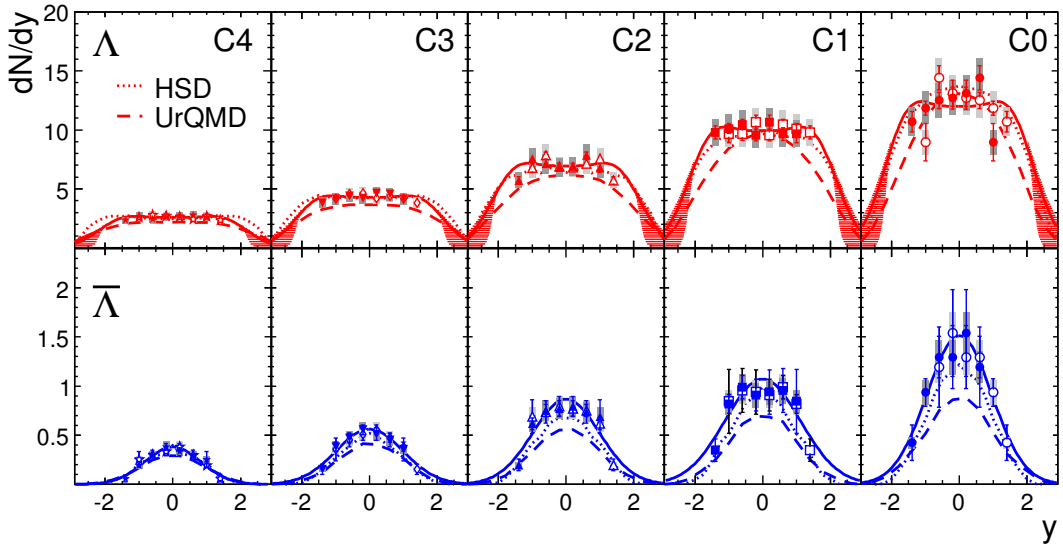

Figure 2: Rapidity spectra of Λ and $\bar{\Lambda}$ hyperons in Pb+Pb collisons at 158A GeV in bins of decreasing centrality C0 - C4. Solid lines are fits to the data points used to extract total yields. Measurements are compared to calculations with the HSD (dotted lines) and UrQMD2.3 (dashed lines) models.

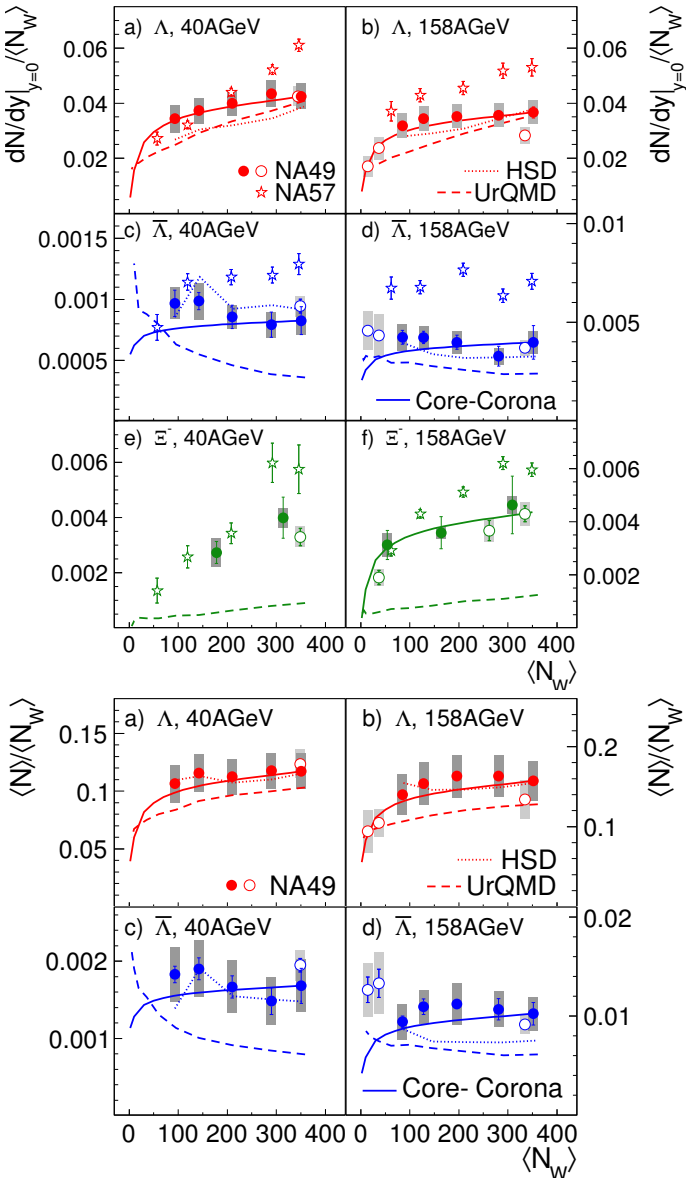

Figure 3: Top: rapidity densities dN/dy divided by the number of wounded nucleons $\langle N_W \rangle$ of Λ, $\bar{\Lambda}$ and Ξ^- at midrapidity for C+C, Si+Si and Pb+Pb collisions at 40A and 158A GeV as a function of $\langle N_W \rangle$. Also shown are results from the NA57 collaboration and calculations with the HSD (dotted line), the UrQMD2.3 (dashed lines) and the core-corona (solid lines) models. Bottom: Total yields $\langle N \rangle$ per $\langle N_W \rangle$.

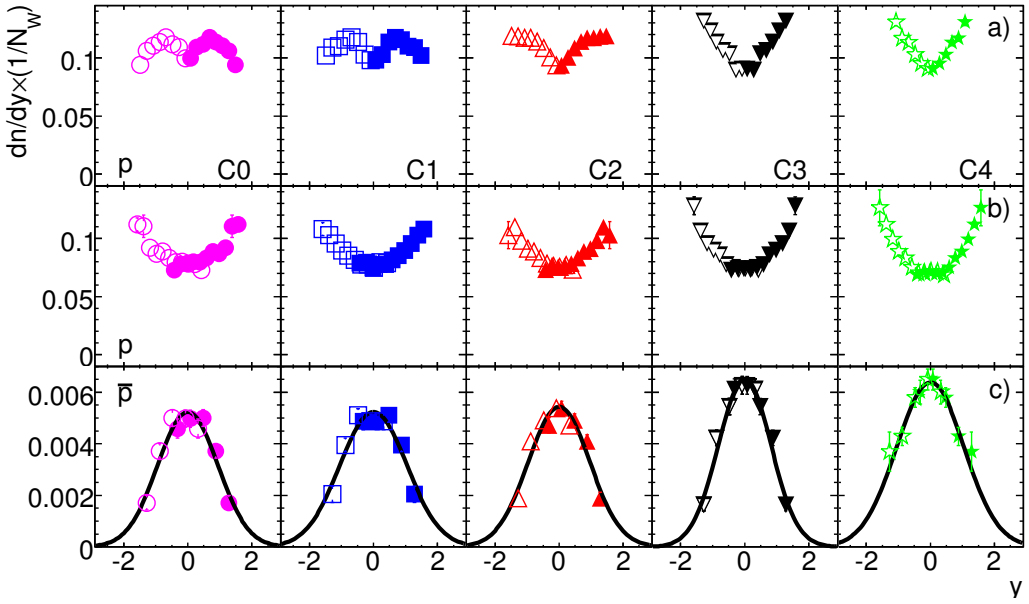

Figure 4: Rapidity spectra of p from 40A GeV (top) and p (center), $\bar{\text{p}}$ (bottom) from 158A GeV Pb+Pb collisions normalised to the number of wounded nucleons $\langle N_W \rangle$ in bins of decreasing centrality C0 - C4. Solid lines are Gaussian fits to the $\bar{\text{p}}$ data points used to extract total yields. (NA49 preliminary)

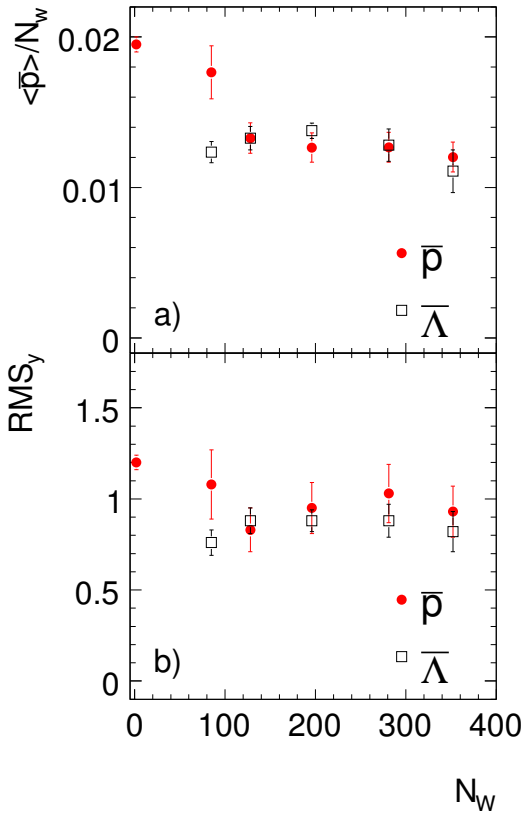

Figure 5: Total multiplicities normalised to the number of wounded nucleons $\langle N_W \rangle$ (top) and RMS$_y$ widths of the rapidity distributions (bottom) for $\bar{\text{p}}$ (dots, NA49 preliminary) and $\bar{\Lambda}$ (squares) in p+p and centrality selected Pb+Pb collisions at 158A GeV.

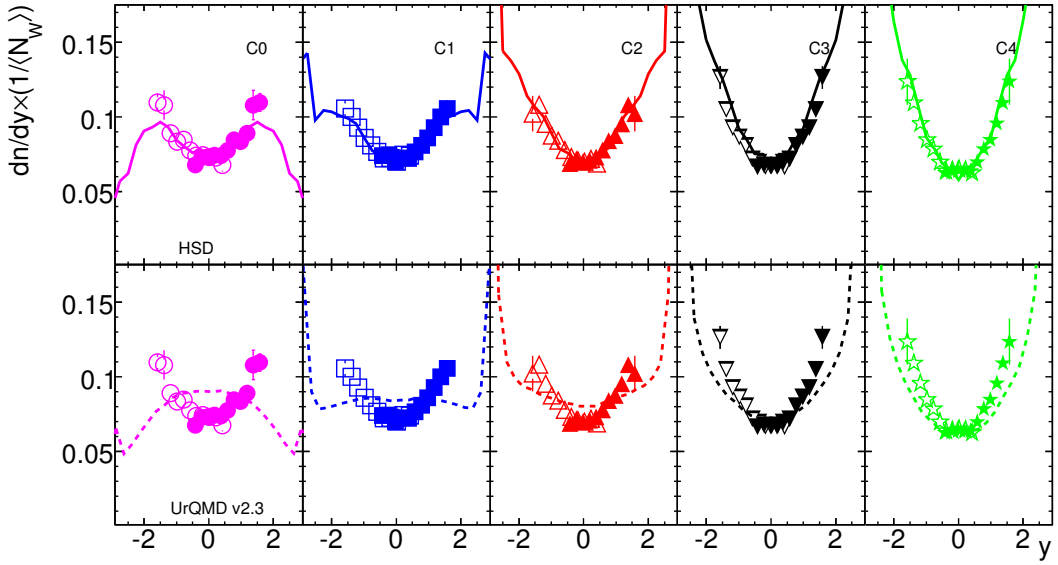

Figure 6: Rapidity distribution of net protons (p - $\bar{\text{p}}$) in Pb+Pb collisions at 158A GeV energy normalised to the number of wounded nucleons $\langle N_W \rangle$ for 5 centrality intervals. Calculations with the HSD (solid curve) and UrQMD2.3 (dashed curve) models are shown for comparison. (NA49 preliminary)

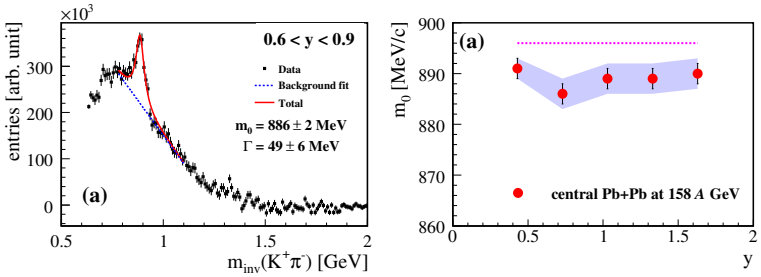

Figure 7: Left: Invariant mass distribution of $K^+\pi^-$ in the rapidity region $0.6 < y < 0.9$ after subtraction of mixed-pair background. The fitted polynomial background is shown by the dashed curve, the sum of fitted polynomial background and signal Breit-Wigner function by the solid curve. Right: Fitted mass values m_0 of the $K^*(892)^0$ mass peak versus center-of-mass rapidity y. Dots show the fitted values and the band indicates the quadratic sum of statistical and systematic uncertainties. (NA49 preliminary)

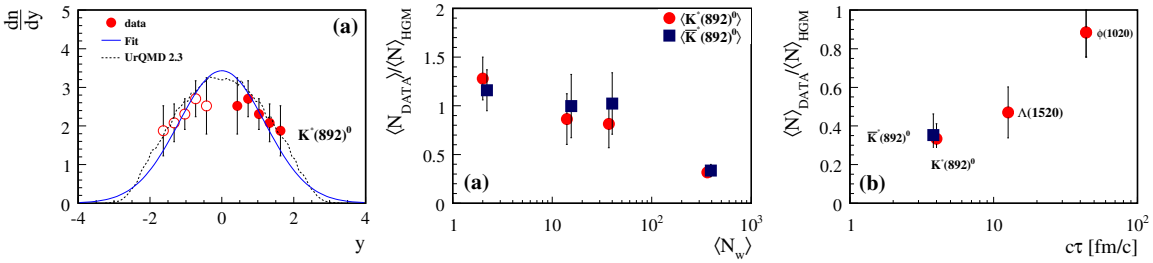

Figure 8: Left: Distribution of rapidity for $K^*(892)^0$ in central Pb+Pb collisions at 158A GeV. Measurements are shown by full dots, open dots were obtained by reflection around mid-rapidity. Full curve depicts a Gaussian fit, predictions of the UrQMD2.3 model are shown by the dotted curve. The bars show the quadratic sum of statistical and systematic errors. Center: Ratio of measured total yields of $K^*(892)^0$ (dots) and $\bar{K}^*(892)^0$ (squares) to statistical hadron gas model predictions versus size of the collision system. Right: Ratio of measured yield to the statistical hadron gas model prediction for $K^*(892)^0$ (dot), $\bar{K}^*(892)^0$ (square), $\Lambda(1520)$ and ϕ meson versus the lifetime $c\tau$ of the resonance state. (NA49 preliminary)

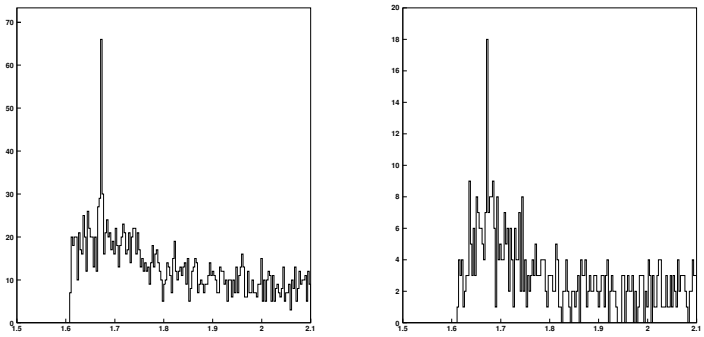

Figure 9: Invariant mass spectra for ΛK^- for $|y| < 0.75$ (left) and $\bar{\Lambda} K^+$ for $|y| < 0.25$ in inelastic p+p collisons at 158 GeV/c. (NA49 preliminary)

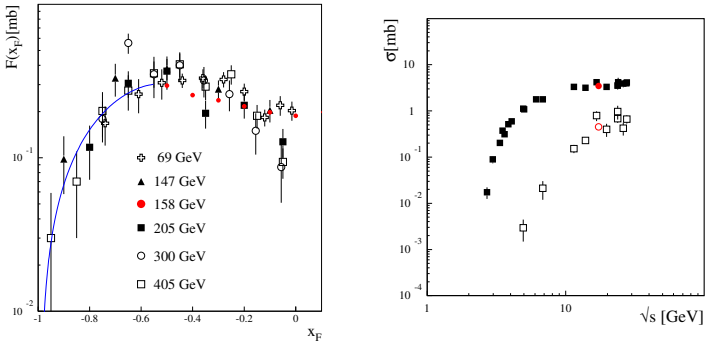

Figure 10: Λ and $\bar{\Lambda}$ production in inelastic p+p collisons at 158 GeV/c. Left: Invariant Λ cross section as a function of x_F at various energies compared to the NA49 measurements. Right: Total inclusive cross sections as a function of $\sqrt{s}$ for Λ (full symbols) and $\bar{\Lambda}$ (empty symbols). The results of NA49 are given by circles, data from other experiments by squares. (NA49 preliminary)

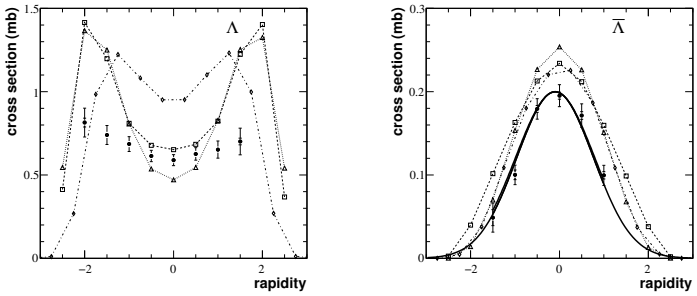

Figure 11: Left: Rapidity distribution for Λ production in inelastic p+p collisons at 158 GeV/c. Right: Rapidity distribution for $\bar{\Lambda}$ production in inelastic p+p collisons at 158 GeV/c. The solid curve depicts a Gaussian fit from which the total yield of $\bar{\Lambda}$ was determined. Data are plotted as dots, model predictions by VENUS (squares), Fritjof (triangles) and UrQMD2.3 (diamonds) are shown for comparison. (NA49 preliminary)

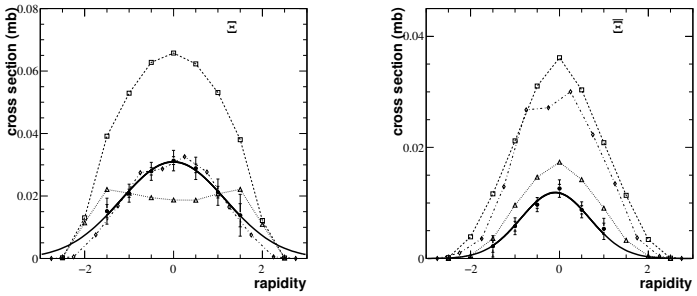

Figure 12: Left: Rapidity distribution for Ξ production in inelastic p+p collisons at 158 GeV/c. Right: Rapidity distribution for $\bar{\Xi}$ production in inelastic p+p collisons at 158 GeV/c. The solid curves depict Gaussian fits from which the total yield of Ξ and $\bar{\Xi}$ were determined. Data are plotted as dots, model predictions by VENUS (squares), Fritjof (triangles) and UrQMD2.3 (diamonds) are shown for comparison. (NA49 preliminary)

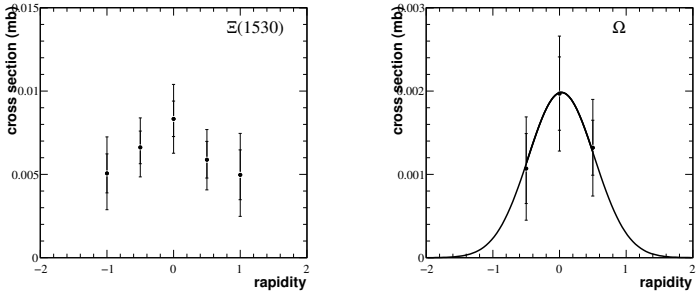

Figure 13: Left: Rapidity distribution for $\Xi(1530)$ production in inelastic p+p collisons at 158 GeV/c. Right: Rapidity distribution for Ω production in inelastic p+p collisons at 158 GeV/c. The solid curve depicts a Gaussian fit from which the total yield of Ω was determined. (NA49 preliminary)